Talanta 83 (2011) 1507–1514

Contents lists available at ScienceDirect

Talanta

journal homepage: www.elsevier.com/locate/talanta

Bicontinuous gyroidal mesoporous carbon matrix for facilitating protein electrochemical and bioelectrocatalytic performances

Chunping You[a,b], Xuewu Yan[a], Jilie Kong[a], Dongyuan Zhao[a], Baohong Liu[a,*]

[a] Department of Chemistry and Key Lab of Molecular Engineering of Polymers of Chinese Ministry of Education, Fudan University, Shanghai 200433, China
[b] State Key Laboratory of Dairy Biotechnology, Technology Center, Bright Dairy and Food Co. Ltd., Shanghai 200436, China

ARTICLE INFO

Article history:
Received 2 August 2010
Received in revised form
18 November 2010
Accepted 18 November 2010
Available online 26 November 2010

Keywords:
Mesoporous materials
Carbon
Glucose oxidase
Myoglobin
Electron transfer
Biosensor

ABSTRACT

A strategy of protein-entrapment in bicontinuous gyroidal mesoporous carbon (BGMC) nanocomposite films is described. Herein, the quasi-reversible electron transfer of redox proteins (such as glucose oxidase and myoglobin) is probed and the associated biocatalytic activity is revealed. The apparent heterogeneous electron transfer rate constant of the immobilized glucose oxidase is up to 9.4 s^{-1}, much larger than those in carbon nanotubes and some conventional mesoporous carbons. The BGMC based glucose biosensor enables the determination of glucose at a potential of 0.6 V (vs. SCE). Its detection limit is 1.0×10^{-5} M (signal-to-noise ratio, S/N = 3), the linear response is up to 7.49 mM and the detection sensitivity is 52.5 nA mM^{-1} Furthermore, a series of BGMCs with different pore sizes is designed and synthesized using sucrose or phenol formaldehyde resin to study the influences of pore sizes and carbon sources on the immobilization of redox proteins and on the heterogeneous electron transfer.

1. Introduction

The combination of biological molecules and novel nanomaterials is of great importance in the process of developing new nanoscale devices for biological, medical and electronic applications. The electrical contacting of redox proteins with electrodes is a subject of extensive research on biosensors. With good conductance and chemical stability, the well-known carbon nanotubes (CNTs) have been increasingly utilized to promote heterogeneous electron transfer (ET) between redox proteins and electrodes [1–5]. When no mediators present, only a few redox proteins performed direct ET at the CNTs-modified electrodes [2–4].

Carbon mesoporous materials (CMMs), a new type of nanostructured materials [6], have recently shown many unique properties and attracted growing interest in diverse fields such as catalyst carriers [7], absorbents and electronic devices [6,8]. As is well known, CNTs are composed of separate or entangled nanotubes, exhibiting a broad distribution in tube diameters. Different from CNTs, CMMs are composed of carbon nanorods with highly ordered arrays, much narrow pore size distributions, large surface areas (up to ca. 2000 $m^2 g^{-1}$) and large porosity (up to ca. 1.5 $cm^3 g^{-1}$). More importantly, CMMs can be easily prepared with tunable pore diameters and rigid structure order via the nanocasting strategy. And such strategy with low cost is free from any impurities if silica 'mold' is fully etched away. All of these advantages make it possible to design the selectivity of supports for biomolecule immobilization, by varying the pore diameter, mesoscopic topology and charge of CMMs.

CNTs and some of CMMs, however, possess only one-dimensional (1D-) or two-dimensional (2D-) ordered framework, resulting in their conductivity anisotropy [9]. As for some three-dimensional (3D-) CMMs replicated from silica template MCM-48 (*e.g.* CMK-1) [6] or FDU-5 [10], the partial displacement of their carbon frameworks leads to the decrease in spatial symmetry and simultaneously the increase in conductivity anisotropy. Thus the above carbon matrixes are limited in achieving a considerably ideal promotion of heterogeneous ET. Besides, though many attempts have been made to immobilize proteins in ordered CMMs [11–14], few reports have focused on the electrochemical biosensing application of large proteins due to the limited pore diameter of CMMs [12,15].

Therefore in this paper, a kind of bicontinuous gyroidal mesoporous carbon (BGMC) was synthesized from KIT-6 silica template, for the purpose of declining the conductivity anisotropy of CMMs. And a strategy was described of protein-entrapped BGMC nanocomposite films. The immobilized redox proteins (glucose oxidase and myoglobin as the models) showed fast electrochemistry and retained the bioactivity to a certain extent. Furthermore, a

* Corresponding author. Tel.: +86 21 65642009; fax: +86 21 65641740.
E-mail address: bhliu@fudan.edu.cn (B. Liu).

0039-9140/$ – see front matter © 2010 Elsevier B.V. All rights reserved.
doi:10.1016/j.talanta.2010.11.041

series of BGMCs of different pore sizes from 2 to 7 nm was synthesized with sucrose or phenol formaldehyde resin as a carbon source to study the influences of pore sizes and carbon sources on the immobilization of redox proteins and on the heterogeneous ET.

2. Experimental

2.1. Materials

Glucose oxidase (GOx, from *Aspergillus niger*, 157,500 units g^{-1}), myoglobin (Mb, from equine heart, 95%), Nafion® perfluorinated ion-exchange resin, 5 wt.% solution and flavin adenine dinucleotide (FAD, 95%) were purchased from Sigma–Aldrich (USA). Ferrocenecarboxylic acid (Fc, 97%) was purchased from Fluka. All other reagents (*e.g.* phenol formaldehyde resin and sucrose) were of analytical grade. Phosphate buffer solutions (PBS, 0.05 M, pH 5.0–8.0) were prepared by mixing the stock solution of NaH_2PO_4 and Na_2HPO_4. The freshly prepared D-glucose ($[\alpha]_D^{20} = 52.5–53.0^\circ$) solution was allowed to come to mutarotation equilibrium by standing overnight. Deionized water was used in all experiments.

2.2. Syntheses of BGMC

The syntheses of BGMC were performed using KIT-6 mesoporous silicas as the template and sucrose [16,17] or phenol formaldehyde (PF) resin [18,19] as the carbon source.

2.3. Preparation of the GOx/BGMC-modified electrode

Prior to coating, a glassy carbon electrode (GCE, 3 mm in diameter) was polished with diamond paper, followed by 0.3, 0.1 and 0.05 μm alumina particles, rinsed thoroughly with deionized water between each polishing step, and successively washed with 1:1 nitric acid, acetone and double distilled water in an ultrasonic bath, respectively. BGMC or 2D-CMM or 3D-CMM was dispersed in 0.05 M PBS containing 0.5% Nafion (pH 7.0) to give a 0.5 mg mL^{-1} homogeneous black suspension. Then, the GCE was coated by casting a drop of 10 μL suspension above and dried under ambient condition. Enzyme immobilization was achieved by matrix adsorption method by immersing the modified GCE into 5 mg mL^{-1} GOx aqueous solution at 4 °C for 48 h. Prior to all measurements, these prepared electrodes were rinsed with buffer solution to remove the non-immobilized proteins. The FAD/BGMC-modified electrode was prepared similarly by immersing BGMC-modified GCE into 0.05–0.1 mg mL^{-1} FAD aqueous solution.

2.4. Apparatus

Electrochemical measurements were preformed with a CHI 1030 electrochemical workstation (CHI, USA) using a three-electrode system, with a modified GCE as the working electrode, a platinum plate as the counter electrode, and a saturated calomel electrode (SCE) as the reference, in a thermostated, stirred electrochemical glass cell containing 10 mL 0.05 M PBS (pH 7.0). All experimental solutions were deoxygenated by bubbling nitrogen through them for 30 min before measurements and maintained under nitrogen atmosphere during measurements. Low-angle X-ray diffraction (XRD), scanning electron microscopy (SEM) and transmission electron microscopy (TEM) experiments were conducted on a German Bruker D4 X-ray diffractometer with Ni-filtered Cu K_α radiation, a Philips XL 30 microscope at an accelerating voltage of 25 kV and a JEOL 2010 microscope at 200 kV, respectively. Nitrogen adsorption/desorption isotherms were measured at 77 K on a Quantachrome Autosorb-1 adsorption apparatus after degassing samples at 453 K for 5 h. Raman spectrum was obtained using a Dilor LabRAM-1B Raman microscope with 532.8 nm excitation.

3. Results and discussion

3.1. Characteristics of BGMC

Scheme 1A shows the structures of silica templates and their responding carbon replicas [20]. With the symmetry of cubic $Ia\bar{3}d$, KIT-6 silica has a framework of two enantiomeric bicontinuous branched self-intersecting volumes separated by an infinite wall analogous to MCM-48 (Scheme 1A, left) [16]. Red and white sections represent left-hand and right-hand spiral rods, respectively (for interpretation of the references to color in this text, the reader is referred to the web version of the article). In contrast to the separate channels of MCM-48 and FDU-5, the two intertwined systems of KIT-6 can be connected through irregular micropores present in the mesoporous walls (Scheme 1A, right) analogous to those in SBA-15 (Scheme S1 in supplementary materials) [21]. Therefore, although the symmetry of MCM-48 and FDU-5 silicas is $Ia\bar{3}d$, their carbon replicas transforms to either tetragonal $I4_1/a$ or lower [6,10] after removal of silicas; while BGMC is a faithful negative replica of $Ia\bar{3}d$ structure from KIT-6 silica [22]. This deduction is confirmed as the following experiments.

TEM images and XRD pattern (Fig. 1A) feature highly ordered 3D-cubic bicontinuous mesostructures of BGMC. It should be noted here that BGMC has an entirely undisplaced mesoscopic gyroidal carbon frameworks and the corresponding space groups might be assigned as pure $Ia\bar{3}d$ [16,17]. Nitrogen adsorption/desorption curve of BGMC shows a typical type-IV isotherm (Fig. 1B), suggesting a uniform mesopore structure. BGMC prepared herein has high Brunauer–Emmett–Teller (BET) surface area of 1241 $m^2\,g^{-1}$, total pore volume of 1.59 $cm^3\,g^{-1}$ and uniform mesopore size of 4.6 nm. Raman spectrum (Fig. 1C) of BGMC exhibits the presence of D-band (1321.2 cm^{-1}) and G-band (1602.28 cm^{-1}). D-band is linked to breathing modes of aromatic rings, ascribed to atomically disordered carbon; while G-band due to the sp^2 C–C stretching is the characteristic feature of ordered graphite carbon, revealing a well-defined graphitized structure of BGMC [23]. Thus the high relative intensity ratio of D-band and G-band ($I_D/I_G = 2.81$) means BGMC contains considerable edge-plane-like defective sites [24,25]. For comparison purpose, 2D-CMM and 3D-CMM replicated from mesoporous silicas SBA-15 [26,27] and FDU-5 [10,28], respectively, are also discussed.

Moreover, a series of BGMCs of different pore sizes ranging from 2 to 7 nm synthesized with sucrose or PF as a carbon source also possesses an $Ia\bar{3}d$ mesoscopic structure. The corresponding XRD patterns, N_2 adsorption/desorption curves and pore size distributions are shown in Fig. 1(D)–(F). It should be noted that for the BGMC synthesized with PF, the partial-filling effect may result in discontinuous filling of the channels and the bimodal pore size distribution; and additionally, the macromolecular effect may result in symmetry decline due to the elimination of the linkers between two enantiomeric rods after removal of silica [19]. It is especially remarkable for the as-synthesized BGMC with a larger pore size of 7.3 nm, which can be observed through the display of [1 1 0] reflection peak in XRD pattern, two hysteresis loops in N_2 adsorption/desorption curves and the bimodal pore size distribution.

The schematic illustration of GOx/BGMC electrode is shown in Scheme 1B. The BGMC was readily dispersed and solubilized in Nafion solution and then deposited on the surface of GCE. SEM image (Fig. S1 in supplementary materials) shows the layered-rock-like BGMC particles (insets top) and BGMC dispersed in Nafion film.

The electrical conductivity of BGMCs can be investigated by the cyclic voltammograms (CVs, Fig. S2 in supplementary mate-

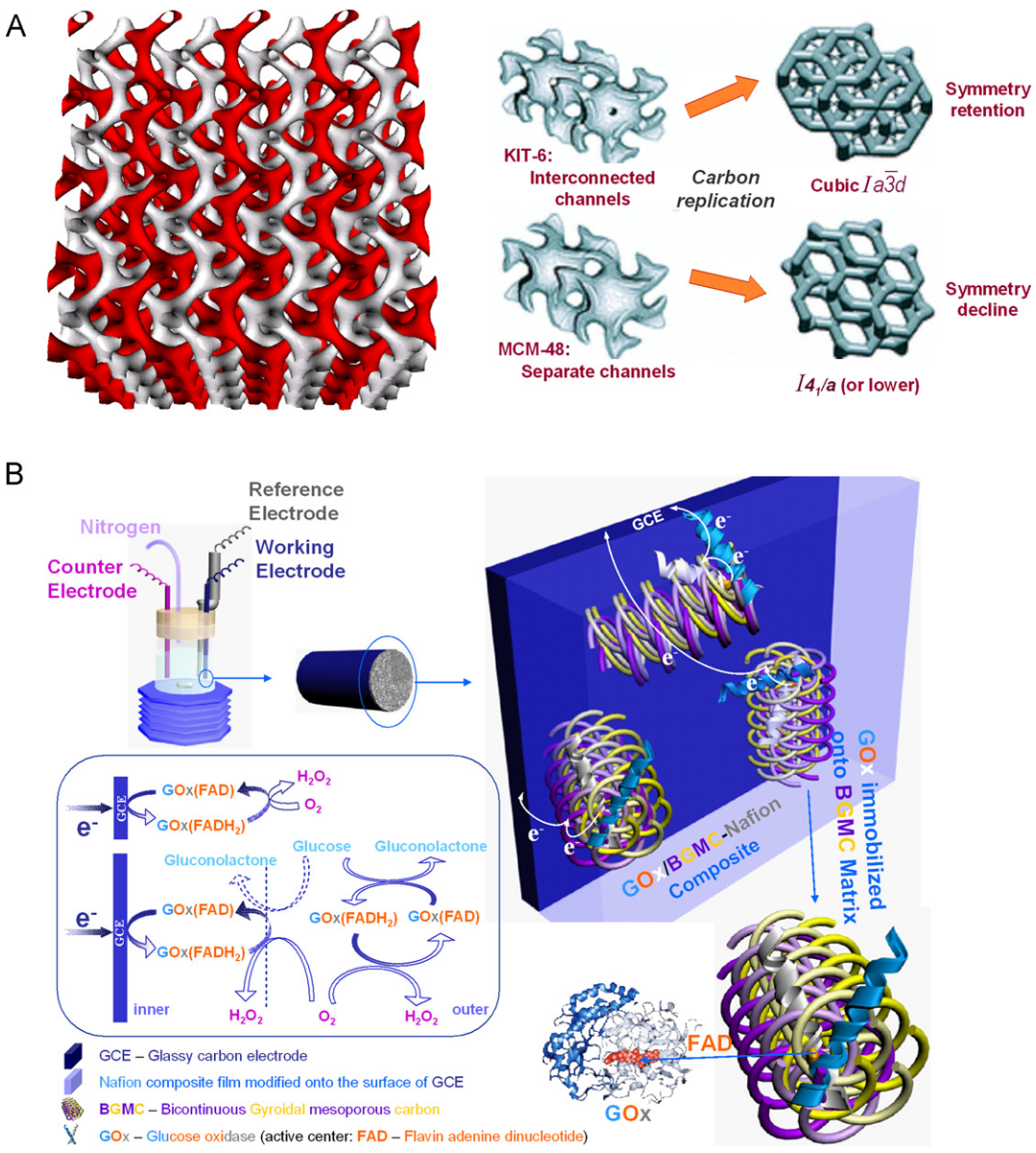

Scheme 1. (A) Structure scheme of $Ia\bar{3}d$ silicas and their corresponding carbon replicas (some portion of this scheme is cited from Ref. [20]). (B) Schematic diagram of the assembly, electron transfer and bioelectrocatalytic processes of GOx/BGMC electrode.

rials) of the BGMC-modified GCEs with Fc as a redox probe. One pair of reversible redox waves of Fc is observed with a formal potential of around 0.326 V, indicating the mutual conversion of ferrocene/ferricinium redox couple at the modified electrode [29]. Under the condition of the similar pore size, it can be concluded from Table S1 (see supplementary materials) that the peak potential separation (ΔE_p) at BGMC/GCE is smaller than that at 2D-CMM/GCE and 3D-CMM/GCE (Table S1A); and ΔE_p at BGMC/GCE with sucrose as a carbon source is smaller than that at BGMC/GCE with PF as a carbon source (Table S1B), indicating the enhanced electrical conductivity of BGMCs resulting from the decreasing conductivity anisotropy with the increasing ordered dimensions and symmetry. It is reported that graphite is a kind of anisotropic solid. The conductivity of carbon materials remarkably depends on the migration [3] of the nonlocalized π-electrons of graphite layers. The conductivity along the growth direction of pore walls is much lower than that along the extended direction of graphite layers [9]. Therefore, the increase in ordered dimensions from 2D to 3D and the increase in symmetry from $I4_1/a$ to $Ia\bar{3}d$ lead to the decrease in conductive anisotropy, providing an increasing total electrical conductivity.

In addition, the apparent electroactive surface area of BGMC/GCE can be obtained by chronoamperometry method according to the Cottrell equation to be $1.69 \pm 0.12\,cm^2$ [30], much higher than that of bare GCE ($0.11 \pm 0.01\,cm^2$) and the apparent geometric surface area of bare GCE ($0.07\,cm^2$). It means that the BGMC-modified electrode can offer more electroactive sites for protein-loading and electron-transferring, providing a higher detection sensitivity and a larger current signal.

3.2. Electrochemistry of proteins immobilized on BGMC and related electron transfer kinetics

Fig. 2A shows the CV of the assembled GOx on the BGMC-modified electrode (pore size: 4.6 nm, carbon source: sucrose). A pair of well-defined redox peaks emerges between −0.46 and −0.43 V at GOx/BGMC electrode (Fig. 2A(a)), similar with redox peaks at FAD/BGMC electrode (Fig. 2A(b)); while no redox peak

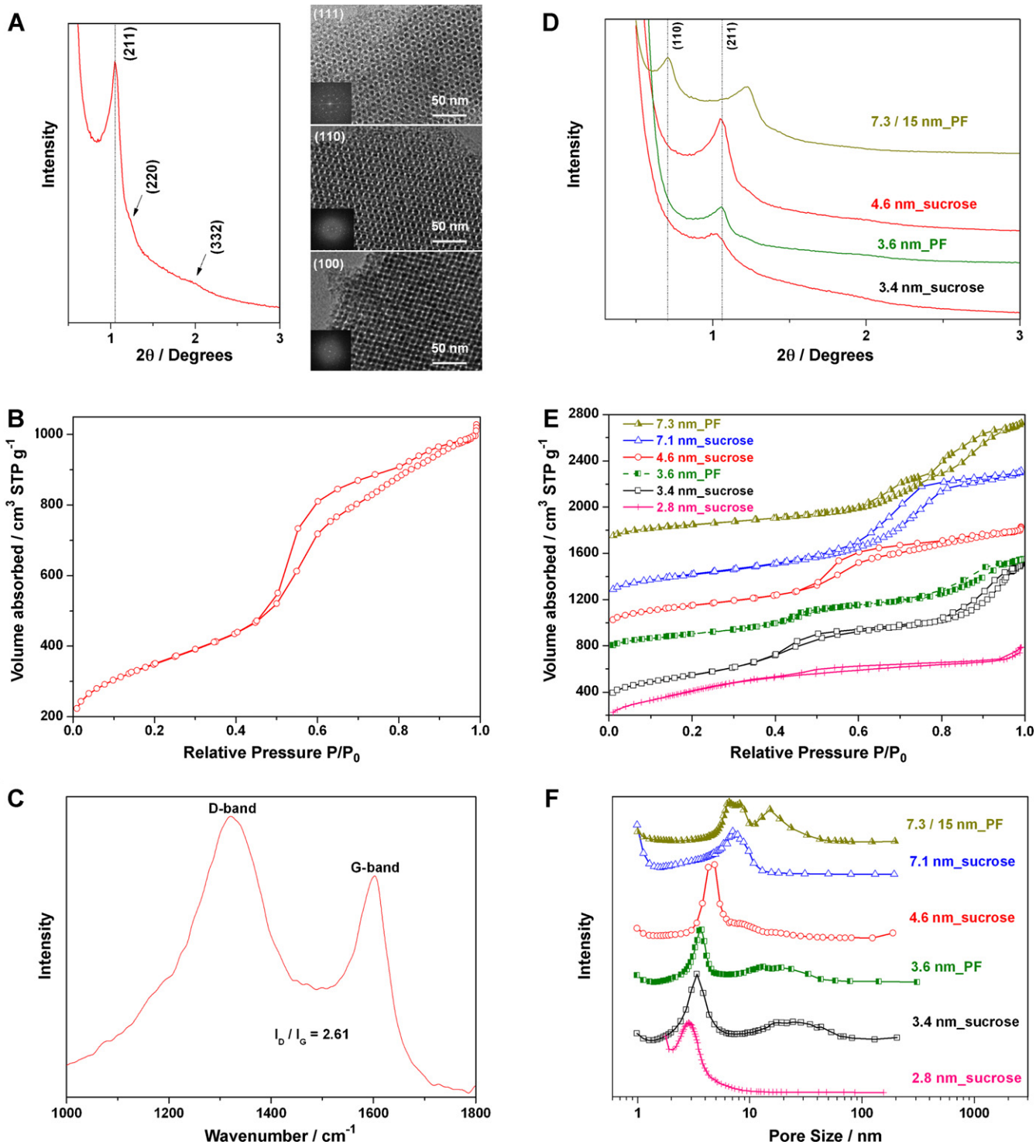

Fig. 1. (A) XRD pattern (left), TEM images viewed along the [1 1 1], [1 1 0], [1 0 0] directions (right, from top to bottom) and the corresponding Fourier diffractograms (right insets), (B) Nitrogen adsorption–desorption isotherm, (C) Raman spectrum of BGMC synthesized with sucrose (pore size: 4.6 nm), (D) XRD patterns, (E) Nitrogen adsorption–desorption isotherms and (F) corresponding pore size distributions of BGMCs synthesized with sucrose or PF.

is observed for the bare underlying BGMC or Nafion electrode (Fig. 2A(c) and (d)). For GOx/BGMC GCE, the formal potential ($E^{0\prime}$) is −0.437 V at a scan rate of 10 mV s^{-1}, close to −0.441 V for FAD/BGMC GCE; while ΔE_p is 18 mV, smaller than that of FAD/BGMC GCE (43 mV). It displays the electrochemical conversion of the immobilized GOx between GOx (FAD) and GOx ($FADH_2$) [31,32], as shown in Scheme 1B. The effect of scan rate on the electrochemical response of immobilized GOx is shown in Fig. 2B. The peak currents increase linearly with the increase in the scan rates from 10 to 200 mV s^{-1}, and the cathodic and anodic peak potentials of the immobilized GOx show shift in negative and positive directions, respectively, indicating a typical surface-confined redox behavior.

Regarding the immobilizing capacities of proteins on BGMC-modified electrodes, integration of the areas under the cathodic peak (Q) of the CVs shown in Fig. 2A gives GOx average surface

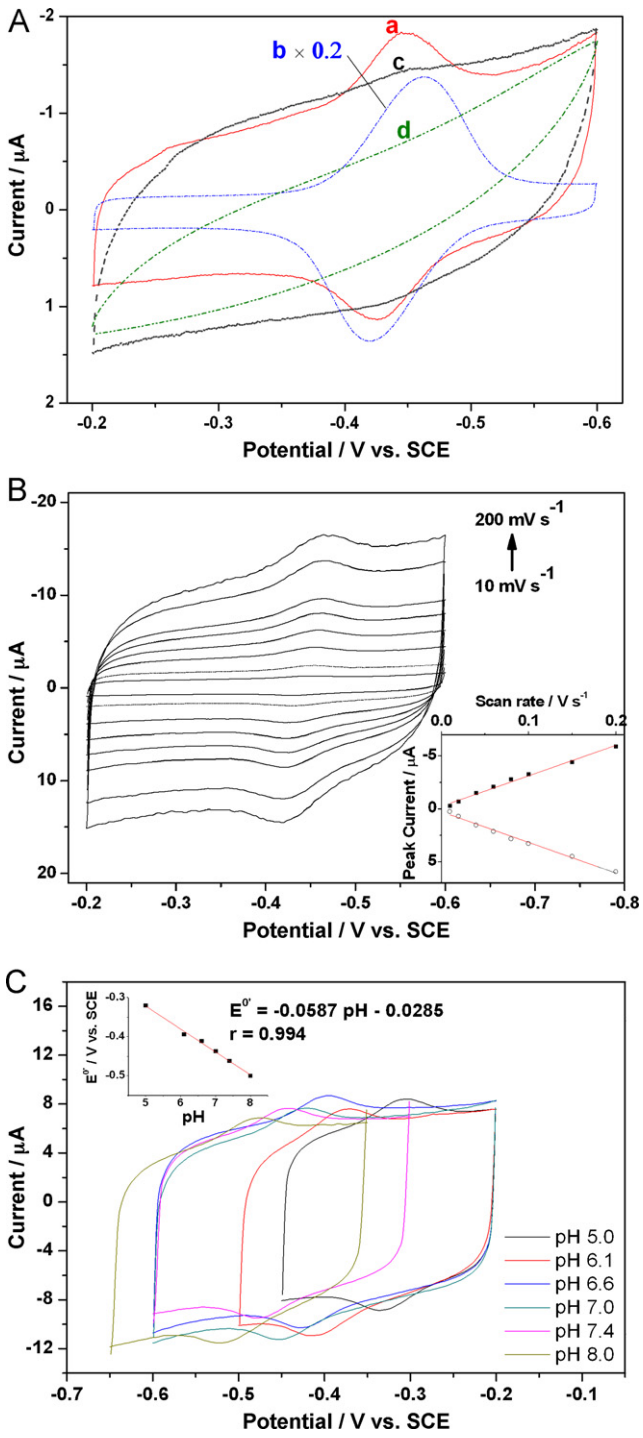

Fig. 2. (A) CVs of GOx/BGMC (a), FAD/BGMC (b), BGMC (c) and Nafion (d) electrodes in pH 7.0 protein-free PBS at a scan rate of 10 mV s^{-1} at 30 °C. (B) CVs of GOx/BGMC electrode in pH 7.0 protein-free PBS at the scan rate of 10, 20, 40, 60, 80, 100, 150, and 200 mV s^{-1} at 30 °C and plots of cathodic and anodic peak current versus scan rates for GOx/BGMC electrode (inset). (C) CVs of GOx/BGMC electrode in a series of protein-free PBS of different pH values at a scan rate of 50 mV s^{-1} at 30 °C and plot of formal potentials versus pH values for GOx/BGMC electrode (inset).

coverage (Γ) [33] according to Eq. (1):

$$\Gamma = \frac{Q}{nFA} \quad (1)$$

where n is the number of the electrons transferred, F is the Faraday constant and A is the electrode area. The evaluated GOx surface coverage of BGMC-modified electrode is 1.8×10^{-10} mol cm^{-2} (Table 1A), much larger than those of the electrodes modified with gold nanoparticles (9.8×10^{-12} mol cm^{-2}) [34], GOx/CdS (1.54×10^{-11} mol cm^{-2}) [35], GOx/SWCNT/PDDA (2.35×10^{-11} mol cm^{-2}) [36] and GOx/SWCNT/chitosan (1.3×10^{-10} mol cm^{-2}) [37]. The Γ value of GOx/BGMC is 61 times as large as the theoretical value of full-packed monolayer (2.97×10^{-12} mol cm^{-2}), assuming the long axis of GOx molecule (5.5 nm × 7.0 nm × 8.0 nm [38]) parallel to the electrode surface. The result indicates a multilayer-adsorption of GOx attributed to the enhanced electroactive surface area of the modified GCE compared with the bare GCE.

The effect of solution pH on the formal potentials of GOx/BGMC electrodes at a scan rate of 50 mV s^{-1} was also investigated in Fig. 2C. The formal potentials depend linearly on the pH value in the range of 5.0–8.0 with a slope of (-58.7 ± 2.1) mV pH^{-1} ($r = 0.994$), which are close to the theoretical value of -59.2 mV pH^{-1} corresponding to the conversion between GOx(FAD) and GOx($FADH_2$) [34,35], indicating a two-electron coupled with two-proton reaction process as Eq. (2) [33].

$$GOx(FAD) + 2e^- + 2H^+ \rightleftharpoons GOx(FADH_2) \quad (2)$$

For GOx is a redox enzyme whose redox active centre, *i.e.* the ($FAD/FADH_2$) cofactor, is embedded deeply within the glycoprotein and hence direct ET cannot easily be achieved on conventional electrodes. Recently, it has been reported that GOx could be immobilized onto CNTs and exhibited the direct ET behavior [3]. The fact that the fast quasi-reversible ET of GOx can be probed in the current work, in our opinion, may be mainly contributed to high surface area and good electroactive property of BGMC. As discussed in Section 3.1, the high surface area of BGMC provides a high apparent electroactive surface area and a favorite microenvironment for the immobilized proteins, meeting the requirement of achieving high capacity for protein assembly and enhancing the electrochemical response. The considerable edge-plane-like defective sites contribute the enhanced catalytic activity [24,25]. In addition, the decreasing conductivity anisotropy and the high electrical conductivity also offer great promise for BGMC to facilitate electron communication between entrapped GOx and the electrode.

To explore the efficiency of BGMC acting as an electron promoter, the kinetic heterogeneous ET for the GOx/BGMC electrode was studied. The ΔE_p of GOx/BGMC (18 mV) is obviously smaller than those of GOx/2D-CMM (33 mV) and GOx/3D-CMM (28 mV) (as shown in Table 1A), and further smaller than that of GOx/1D-SWNTP (43 mV) [3]. The above results indicate an increasingly quasi-reversible redox process with the increasing total conductive efficiency of carbons resulting from the increase in the ordered dimensions and the decrease in the conductivity anisotropy. The apparent heterogeneous ET rate constant k^0_{et}, was determined from the scan rate dependence of ΔE_p using the method of Laviron [39]. The deduced k^0_{et} value is 9.4 s^{-1} for GOx/BGMC-modified GCE, larger than 3.9 and 4.2 s^{-1} for 2D- and 3D-CMM-modified GCEs, respectively (as shown in Table 1A); and even much larger than 1.7 s^{-1} reported for GOx/SWNTP electrodes [3]. It suggests that BGMC is an ideally effective electron promoter to facilitate ET between the adsorbed GOx and the electrode. Just because the conductivity anisotropy declines gradually as the increase in the ordered dimensions and symmetry from 2D-CMM to 3D-CMM and finally to BGMC, the ET rate gradually increases at the above mesoporous carbons-modified electrodes.

The immobilized Mb onto the above mesoporous carbon matrices shows the similar ET properties and trend (Fig. S3 and Table S2 in supplementary materials), confirming the above observation for GOx.

Table 1
(A) The loading amounts and ET properties of GOx adsorbed on 2D-CMM, 3D-CMM and BGMC of the approximately equal pore size synthesized similarly with sucrose as a carbon precursor (ΔE_p: at 10 mV s^{-1}). (B) The loading amounts and ET properties of GOx immobilized on a series of BGMCs of different pore sizes synthesized with sucrose or PF as a carbon precursor (ΔE_p: at 10 mV s^{-1}). All the electrochemical data are the average values of five parallel measurements.

(A) GOx/CMM	ΔE_p (mV)	$E^{0\prime}$ (mV vs. SCE)	Γ_{GOx} (10^{-10} mol cm^{-2})	$k^0_{et\text{-}GOx}$ (s^{-1})
GOx/2D-CMM $_{(4.2\,nm)}$	33 ± 2	−446 ± 2	1.9 ± 0.1	3.9 ± 0.2
GOx/3D-CMM $_{(4.1\,nm)}$	28 ± 2	−440 ± 2	5.7 ± 0.2	4.2 ± 0.2
GOx/BGMC $_{(4.6\,nm)}$	18 ± 1	−437 ± 1	1.8 ± 0.1	9.4 ± 0.2

(B) BGMC pore size (nm)	$2.8_{\text{-sucrose}}$	$3.4_{\text{-sucrose}}$	$3.6_{\text{-PF}}$	$4.6_{\text{-sucrose}}$	$7.1_{\text{-sucrose}}$	$7.3_{\text{-PF}}$
BET ($m^2\,g^{-1}$)	1472	1410	1066	1241	1116	1048
Mesopore volume ($cm^3\,g^{-1}$)	1.22	2.1	1.47	1.59	1.87	1.82
Micropore volume ($cm^3\,g^{-1}$)	0	0	0.11	0.1	0.04	0.15
$\Delta E_{p\text{-}GOx}$ (mV)	28 ± 1	25 ± 2	25 ± 3	18 ± 1	18 ± 2	22 ± 2
$E^{0\prime}$-GOx (mV vs. SCE)	−440 ± 1	−438 ± 1	−441 ± 1	−437 ± 1	−437 ± 1	−441 ± 1
Γ_{GOx} (10^{-10} mol cm^{-2})	2.0 ± 0.1	2.0 ± 0.2	1.7 ± 0.1	1.8 ± 0.1	1.7 ± 0.1	1.8 ± 0.1
$k^0_{et\text{-}GOx}$ (s^{-1})	3.4 ± 0.1	5.7 ± 0.2	4.1 ± 0.1	9.4 ± 0.2	7.6 ± 0.1	5.9 ± 0.3

3.3. Influences of pore sizes of BGMC on the immobilization of proteins and on the related electron transfer kinetics

The apparent surface coverage (Table 1B) of proteins immobilized onto BGMC matrices of various pore sizes suggest that the immobilization capacity for proteins is mainly influenced by the close surface areas of BGMCs, not very related to the pore sizes or carbon sources. On the other hand, the immobilized GOx exhibits the smallest ΔE_p and the fastest ET rate in the BGMC matrix with a pore size of 4.6 nm (Table 1B). It is suggested that the pore size of 4.6 nm makes a good match for the size of GOx molecule (5.5 nm × 7.0 nm × 8.0 nm), thus GOx might keep a relatively stable loading state, and the shortest distance between the redox centre and the electrode surface can be achieved, leading to the easiest and fastest ET. The hypothesis can be verified by the experimental results of another protein. Mb molecule is smaller than GOx. The immobilized Mb achieves the smallest ΔE_p and the fastest ET rate through the BGMC with a smaller pore size of 2.8 nm (Table S3), which makes a good match for the size of Mb molecule (2.1 nm × 3.5 nm × 4.4 nm).

3.4. Influences of carbon sources of BGMC on the immobilization of redox proteins and on the related ET

As discussed in Section 3.3, the immobilization capacity for proteins is mainly influenced by the surface area of BGMC, not very related to the pore size or the carbon source.

When the pore sizes are similar, Table 1B shows the smaller ΔE_p and higher ET rate of GOx immobilized onto the BGMC matrix synthesized with sucrose than with PF as a carbon source. It can be concluded that BGMC synthesized with sucrose possesses a higher electrical conductivity and electro-catalytic property as discussed in Section 3.1.

3.5. Bioelectrocatalytic application of the GOx/BGMC-modified electrode

$$GOx(FAD) + \text{glucose} \rightarrow GOx(FADH_2) + \text{gluconolactone} \quad (3)$$

$$GOx(FADH_2) + O_2 \rightarrow GOx(FAD) + H_2O_2 \quad (4)$$

$$GOx(FAD) + 2e^- + 2H^+ \rightarrow GOx(FADH_2) \quad (5)$$

$$2H_2O_2 \rightarrow O_2 + 2H_2O + 2e^- \quad (6)$$

The enzyme activity of the fabricated GOx/BGMC electrode was investigated in nitrogen-saturated and air-saturated PBS, respectively, as shown in Fig. 3. Both of glucose and O_2 can behave as the substrates of GOx [32]. They can react with GOx as Eqs. (3) and (4), respectively. With the addition of glucose into the N_2-saturated PBS (Fig. 3A), the cathodic current of GOx(FAD)/GOx($FADH_2$) redox couple decreases weakly. However, because of the participation of O_2 in air-saturated PBS, the cathodic current of GOx(FAD)/GOx($FADH_2$) redox couple dramatically increases (red curve in Fig. 3B) compared with in the N_2-saturated PBS (black curve in Fig. 3A and B), while anodic current decreases as Eqs. (4) and (5) (for interpretation of the references to color in this text, the reader is referred to the web version of the article). With the addition of air-saturated glucose into the PBS, the dissolved O_2 increases, resulting in the continuous increase in the cathodic current (Fig. 3B). When the concentration of glucose is higher, the cathodic current decreases slowly with the increase in glucose and achieves to equilibrium (Fig. 3C), similar to Fig. 3A. While no such obvious changes occur to FAD/BGMC electrode under the same conditions (not shown). It can be deduced that the immobilized GOx molecules retain their bioactivity to a certain degree. Compared with glucose, it is more accessible for O_2 to approach the active centre of the inner immobilized GOx. Thus the cathodic current dramatically increases with the increase in dissolved O_2, while changes weakly with the increase in glucose. As Scheme 1B shown, glucose mainly acts with the outer immobilized GOx; while both of outer GOx($FADH_2$) reduced by glucose and inner GOx($FADH_2$) generated by electrochemical reduction on the electrode surface consume the dissolved O_2. Therefore, with the addition of glucose into the air-saturated PBS, the cathodic current increases when glucose concentration is lower, then decreases when glucose concentration is higher, and finally the competition between biocatalytic glucose oxidation and biocatalytic O_2 reduction achieves equilibrium. These results are similar to those in the reported literature [32].

Moreover, the glucose biosensor based on the GOx/BGMC electrode was prepared to detect glucose in PBS. As expressed by Eqs. (3), (4) and (6), in the air-saturated PBS, O_2 is acted as a mediator to facilitate the ET between GOx and the electrode, and the glucose can be measured indirectly by detecting the generated H_2O_2 during the oxidation of glucose [40]. As shown in Fig. 3D, the increased current is proportional to the glucose concentration at 0.6 V and the linear response is observed up to 7.49 mM (correlation coefficient, 0.995), equivalent to the level of glucose in blood. The detection limit is 1.0×10^{-5} M (signal-to-noise ratio, S/N = 3) and the detection sensitivity is 52.5 nA mM^{-1}. The corresponding apparent Michaelis–Menten constant k_m^{app} can be evaluated from Lineweaver–Burk equation [41] to be 2.77 mM, which is smaller that 8.2 mM for GOx/CNT/chitosan [42] and 8.5 mM for GOx/SWCNHs/Nafion [43], indicating that the proposed enzyme electrodes exhibit a higher affinity for glucose and the immobilized GOx retains a higher enzymatic activity. The fabricated GOx/BGMC electrodes were stored under 4 °C to investigate the reproducibility and stability. The relative standard deviation (RSD) values of the amperometric responses at 0.6 V to 6 times successive addi-

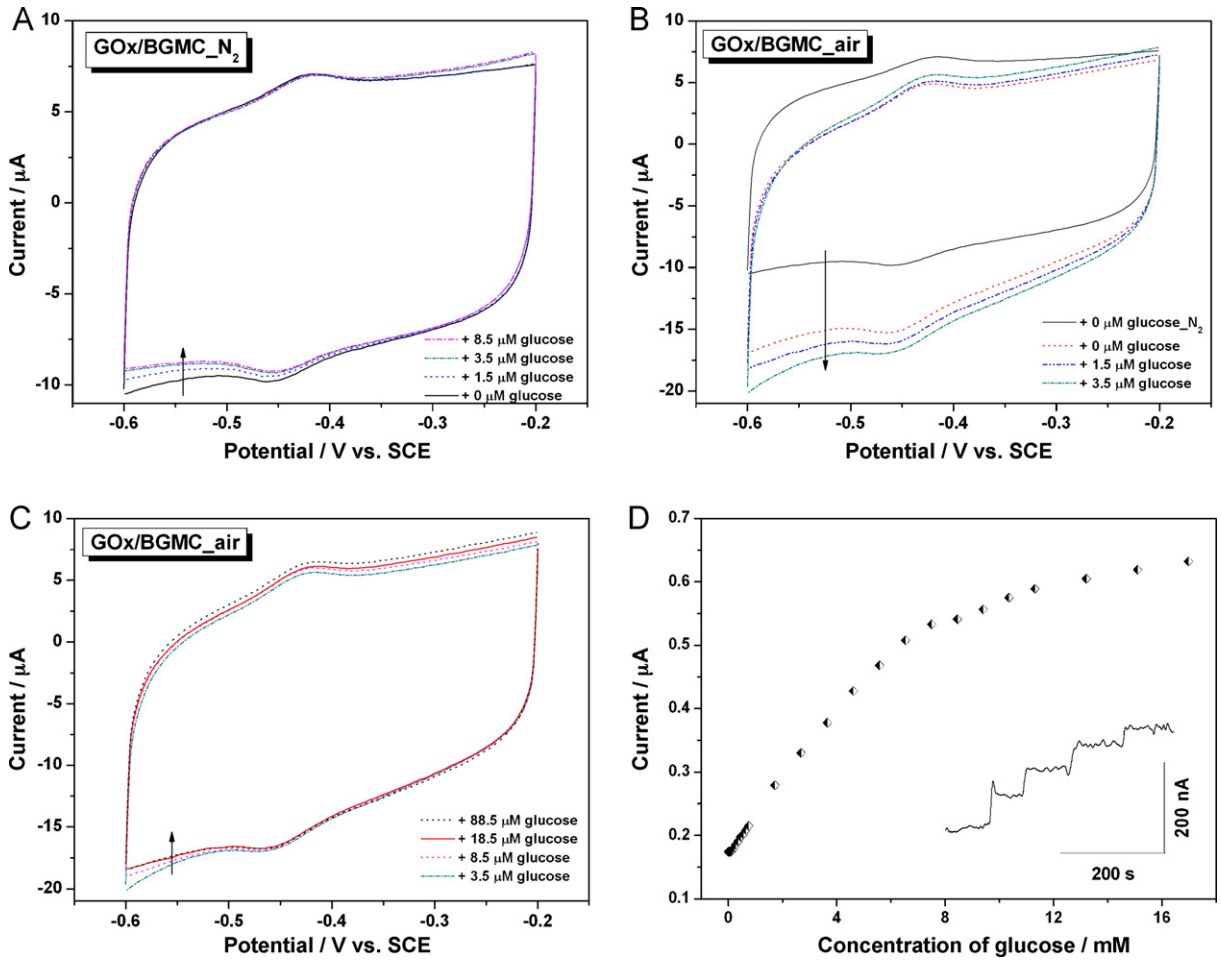

Fig. 3. CVs of GOx/BGMC electrode at a scan rate of 50 mV s^{-1} in the (A) N_2-saturated, and (B and C) air-saturated PBS (pH 7.0) before and after successive additions of glucose at 30 °C. (D) The calibration curve for the electrocatalysis of glucose and the dynamic responses (inset) of the fabricated GOx/BGMC electrode to successive additions of glucose in the air-saturated PBS (pH 7.0) at the applied potential of 0.6 V.

tions of 1.0 mM glucose are 6.8%. 95% of the initial current response is maintained after 30 days, indicating considerable stability of the GOx/BGMC sensor.

4. Conclusions

The potential application of mesoporous carbon has been shown in the bioelectrochemical field. Highly ordered 3D-mesoporous carbon, i.e. bicontinuous gyroidal mesoporous carbon matrices with tailored pore size, have been successfully prepared and introduced to the bioelectrochemical study. Same as the general mesoporous carbons, such materials are suitable candidates for the immobilization of proteins and the promotion of heterogeneous electron transfer. In contrast with CNTs and conventional CMMs, BGMC can more effectively enhance the heterogeneous electron transfer. Besides, it is expectable that the pore diameter and structural topologies (such as tubular, caged nanopores) can be readily tuned to match the dimensional sizes of diverse biomolecules and promote heterogeneous electron transfer. Furthermore, enzyme molecules assembled on BGMC still exhibit high bioactivity to a large extent. All these properties make BGMC valuable in the understanding of the electrochemistry of redox proteins and open a new avenue for the development of carbon-based electrochemical biosensors.

Acknowledgements

This work was supported by the NNSF of China (20775016), Shanghai Shuguang 06SG02 and Leading Academic Discipline Project B108, B109.

Appendix A. Supplementary data

Supplementary data associated with this article can be found, in the online version, at doi:10.1016/j.talanta.2010.11.041.

References

[1] B.R. Azamian, J.J. Davis, K.S. Coleman, C.B. Bagshaw, M.L.H. Green, J. Am. Chem. Soc. 124 (2002) 12664.
[2] M.C. Weigel, E. Tritscher, F. Lisdat, Electrochem. Commun. 9 (2007) 689.
[3] A. Guiseppi-Elie, C.H. Lei, R.H. Baughman, Nanotechnology 13 (2002) 559.
[4] J.J. Gooding, R. Wibowo, J.Q. Liu, W.R. Yang, D. Losic, S. Orbons, F.J. Mearns, J.G. Shapter, D.B. Hibbert, J. Am. Chem. Soc. 125 (2003) 9006.
[5] J. Wang, M. Musameh, Y.H. Lin, J. Am. Chem. Soc. 125 (2003) 2408.
[6] R. Ryoo, S.H. Joo, S. Jun, J. Phys. Chem. B 103 (1999) 7743.
[7] S.H. Joo, S.J. Choi, I. Oh, J. Kwak, Z. Liu, O. Terasaki, R. Ryoo, Nature 412 (2001) 169.
[8] S. Yoon, J.W. Lee, T. Hyeon, S.M. Oh, J. Electrochem. Soc. 147 (2000) 2507.
[9] H.F. Yang, Y. Yan, Y. Liu, F.Q. Zhang, R.Y. Zhang, Y. Meng, M. Li, S.H. Xie, B. Tu, D.Y. Zhao, J. Phys. Chem. B 108 (2004) 17320.
[10] T. Wang, X.Y. Liu, D.Y. Zhao, Z.Y. Jiang, Chem. Phys. Lett. 389 (2004) 327.
[11] A. Vinu, C. Streb, V. Murugesan, M. Hartmann, J. Phys. Chem. B 107 (2003) 8297.
[12] M. Hartmann, A. Vinu, G. Chandrasekar, Chem. Mater. 17 (2005) 829.

[13] H. Takahashi, B. Li, T. Sasaki, C. Miyazaki, T. Kajino, S. Inagaki, Chem. Mater. 12 (2000) 3301.
[14] Y. Mastai, S. Polarz, M. Antonietti, Adv. Funct. Mater. 12 (2002) 197.
[15] J. Lee, K. Sohn, T. Hyeon, J. Am. Chem. Soc. 123 (2001) 5146.
[16] F. Kleitz, S.H. Choi, R. Ryoo, Chem. Commun. (2003) 2136.
[17] T.W. Kim, F. Kleitz, B. Paul, R. Ryoo, J. Am. Chem. Soc. 127 (2005) 7601.
[18] Y.P. Lin, H.P. Lin, D.W. Chen, H.Y. Liu, H.S. Teng, C.Y. Tang, Mater. Chem. Phys. 90 (2005) 339.
[19] L. Zhou, H.Q. Li, C.Z. Yu, X.F. Zhou, J.W. Tang, Y. Meng, Y.Y. Xia, D.Y. Zhao, Carbon 44 (2006) 1601.
[20] T.W. Kim, L.A. Solovyov, J. Mater. Chem. 16 (2006) 1445.
[21] K.P. Gierszal, T.W. Kim, R. Ryoo, M. Jaroniec, J. Phys. Chem. B 109 (2005) 23263.
[22] Y. Sakamoto, T.W. Kim, R. Ryoo, O. Terasaki, Angew. Chem. Int. Ed. 43 (2004) 5231.
[23] A.C. Ferrari, J. Robertson, Phys. Rev. B 61 (2000) 14095.
[24] M. Zhou, J.D. Guo, L.P. Guo, J. Bai, Anal. Chem. 80 (2008) 4642.
[25] C.E. Banks, T.J. Davies, G.G. Wildgoose, R.G. Compton, Chem. Commun. (2005) 829.
[26] D.Y. Zhao, J.L. Feng, Q.S. Huo, N. Melosh, G.H. Fredrickson, B.F. Chmelka, G.D. Stucky, Science 279 (1998) 548.
[27] S. Jun, S.H. Joo, R. Ryoo, M. Kruk, M. Jaroniec, Z. Liu, T. Ohsuna, O. Terasaki, J. Am. Chem. Soc. 122 (2000) 10712.
[28] X.Y. Liu, B.Z. Tian, C.Z. Yu, F. Gao, S.H. Xie, B. Tu, R.C. Che, L.M. Peng, D.Y. Zhao, Angew. Chem. Int. Ed. 41 (2002) 3876.
[29] X. Chen, J.B. Jia, S.J. Dong, Electroanalysis 15 (2003) 608.
[30] V.R. Taliene, T. Ruzgas, V. Razumas, J. Kulys, J. Electroanal. Chem. 372 (1994) 85.
[31] R. Ianniello, J. Lindsay, A. Yacynych, Anal. Chem. 54 (1982) 1098.
[32] D. Shan, J. Zhang, H.G. Xue, S.N. Ding, S. Cosnier, Biosens. Bioelectron. 25 (2010) 1427.
[33] A.J. Bard, L.R. Faulkner, Electrochemical Methods: Fundamentals and Applications, 2nd ed., John Wiley & Sons, New York, 2001.
[34] S.Q. Liu, H.X. Ju, Biosens. Bioelectron. 19 (2003) 177.
[35] Y.X. Huang, W.J. Zhang, H. Xiao, G.X. Li, Biosens. Bioelectron. 21 (2005) 817.
[36] J. Zhang, M. Feng, H. Tachikawa, Biosens. Bioelectron. 22 (2007) 3036.
[37] Y. Zhou, H. Yang, H.Y. Chen, Talanta 76 (2008) 419.
[38] M. Hartmann, Chem. Mater. 17 (2005) 4577.
[39] E. Laviron, J. Electroanal. Chem. 101 (1979) 19.
[40] J. Wang, Chem. Rev. 108 (2008) 814.
[41] R.A. Kamin, G.S. Wilson, Anal. Chem. 52 (1980) 1198.
[42] Y. Liu, M.K. Wang, F. Zhao, Z.A. Xu, S.J. Dong, Biosens. Bioelectron. 21 (2005) 984.
[43] X.Q. Liu, L.H. Shi, W.X. Niu, H.J. Li, G.B. Xu, Biosens. Bioelectron. 23 (2008) 1887.